JOURNAL OF THERMOPHYSICS AND HEAT TRANSFER
Vol. 6, No. 3, July–Sept. 1992

Solution of the Parabolized Navier-Stokes Equations Using Osher's Upwind Scheme

R. A. Gerbsch* and R. K. Agarwal†
McDonnell Douglas Research Laboratories, St. Louis, Missouri 63166

A new, explicit, finite volume algorithm based on Osher's upwind method is applied to the two-dimensional parabolized Navier-Stokes equations to model hypersonic flows. The algorithm is second-order accurate and employs flux limiters to make the scheme total variation diminishing (TVD). The pressure gradient in the subsonic region is limited in the streamwise direction to maintain a hyperbolic inviscid equation set. Second-order central differencing is applied to the viscous terms and upwind differencing is applied to the inviscid terms in both the subsonic and supersonic portions of the flowfield. The new algorithm is demonstrated by computing four laminar-flow cases; supersonic flow over a flat plate, supersonic flow in a diffuser, hypersonic flow over a 15-deg ramp, and hypersonic flow in a converging inlet. Extensive comparisons of heat transfer, skin friction, and pressure coefficients are made between Osher's and Roe's upwind schemes. For this class of flows, Osher and Roe upwinding yield very similar results.

I. Introduction

DESIGN and analysis of flow about supersonic vehicles is now being accomplished with the aid of the parabolized Navier-Stokes equations (PNS). By using the PNS equations the computational burden can be reduced by an order of magnitude. In recent years, upwinding has been applied to the inviscid flux terms in the PNS equations. Upwinding improved the quality of the solutions and eliminated the necessity of adding damping terms associated with the conventional central-difference algorithms. In computational fluid dynamics four major upwind schemes are used: Engquist and Osher,[1] Roe,[2] Steger and Warming,[3] and van Leer.[4] Steger-Warming splitting is not continuously differentiable across the sonic points where the eigenvalues change sign and, consequently, it has a "glitch" at the sonic point.[5] Van Leer splitting is known to yield smeared contact discontinuities, thus requiring more grid points for resolving viscous shear layers. Roe's scheme has gained wide acceptance for the solution of the PNS and Navier-Stokes (NS) equations. The algorithm is fairly easy to implement and the results, for most flows, are very good. Unfortunately, Roe's scheme does not strictly enforce the entropy condition and expansion shocks are possible.[6–8] PNS schemes[9–12] which have employed Roe upwinding require an entropy correction model.[9,13,14] While entropy correction models do eliminate nonphysical features, they are dissipative and they generally introduce another point into the shock-transition process and increase error in the flowfield. However, Osher's[15] scheme rules out expansion shocks and actually enforces the entropy condition. It is continuously differentiable which provides smoothness in transition points and sharp contact discontinuities/shocks. Thus, in cases where the flow experiences large expansions, Osher's method should prove superior to existing upwind methods which have been applied to the PNS equations. Therefore, this current work involves the application of Osher's scheme to the PNS equations.

Presented as Paper 90-0392 at the AIAA 28th Aerospace Sciences Meeting, Reno, NV, Jan. 8–11, 1990; received Aug. 2, 1990; revision received July 22, 1991; accepted for publication July 23, 1991.

*Research Scientist. Member AIAA.
†Program Director. Associate Fellow AIAA.

II. Governing Equations

The PNS equations are readily obtained from the steady, full Navier-Stokes equations by neglecting the streamwise viscous derivatives. Steady, unseparated, multidimensional flows with a predominant flow direction can be modeled with the PNS equations.

Let $\tilde{p}$, $\tilde{\rho}$, $(\tilde{u}, \tilde{v})$, $\tilde{e}$ and $\tilde{h}$ denote pressure, density, the two Cartesian velocity components, total energy, and total enthalpy, respectively, with the "tilde" indicating dimensional quantities. Let $\tilde{\mu}$ and $\tilde{k}$ be the coefficient of viscosity and heat conduction, respectively. Let the functions $\xi = \xi(x, y)$ and $\eta = \eta(x, y)$ describe the coordinate transformation between the Cartesian system (x, y) and the curvilinear system (ξ, η). For the general transformation ξ_x/J and ξ_y/J are the constant-ξ length projection in the y and x directions, respectively, where the "x" and "y" subscripts denote partial differentiation. Similarly, η_x/J and η_y/J are the constant-η length projection in y and x directions, respectively. For the viscous terms, $\eta_\kappa = (\eta_\kappa/J)J'$, where J' is the inverse of the average area between adjacent cells and κ represents x or y.

In an arbitrary curvilinear coordinate system the parabolized form of the Navier-Stokes equations is obtained as

$$\frac{\partial \boldsymbol{E}}{\partial \xi} + \frac{\partial \boldsymbol{F}}{\partial \eta} = 0 \tag{1a}$$

where

$$\boldsymbol{E} = \frac{\xi_x}{J} E_i + \frac{\xi_y}{J} F_i, \quad \boldsymbol{F} = \frac{\eta_x}{J}(E_i - E_v) + \frac{\eta_y}{J}(F_i - F_v) \tag{1b}$$

The i subscript denotes inviscid flux terms and the v subscript denotes viscous flux terms. The flux terms are given as

$$E_i = [\rho u, \rho u^2 + p, \rho uv, (\rho e + p)u]^T$$

$$F_i = [\rho v, \rho uv, \rho v^2 + p, (\rho e + p)v]^T$$

$$E_v = [0, \tau_{xx}, \tau_{xy}, u\tau_{xx} + v\tau_{xy} - q_x]^T$$

$$F_v = [0, \tau_{xy}, \tau_{yy}, u\tau_{xy} + v\tau_{yy} - q_y]^T \tag{1c}$$

The shear stress terms, τ_{xx}, τ_{yy} and τ_{xy}, are given as

$$\tau_{xx} = (2\mu/3Re_\infty)(2\eta_x u_\eta - \eta_y v_\eta),$$

$$\tau_{yy} = (2\mu/3Re_\infty)\,(2\eta_y v_\eta - \eta_x u_\eta)$$

$$\tau_{xy} = (\mu/Re_\infty)\,(\eta_y u_\eta + \eta_x v_\eta) \tag{1d}$$

The heat flux terms, q_x and q_y, are given as

$$q_x = -\frac{\mu}{Re_\infty Pr}\frac{1}{(\gamma-1)M_\infty^2}\eta_x T_\eta$$

$$q_y = -\frac{\mu}{Re_\infty Pr}\frac{1}{(\gamma-1)M_\infty^2}\eta_y T_\eta \tag{1e}$$

Finally, i and h are defined as

$$i = e - \frac{1}{2}(u^2 + v^2), \quad h = e + p/\rho \tag{1f}$$

The Reynolds number is $Re_\infty = \tilde{\rho}_\infty \tilde{U}_\infty \tilde{L}/\tilde{\mu}_\infty$, where $\tilde{U}_\infty$ is the freestream velocity, $\tilde{L}$ is the reference length, $\tilde{\mu}_\infty$ is the freestream viscosity, and $\tilde{\rho}_\infty$ is the freestream density. The freestream Mach number and speed of sound are M_∞ and $\tilde{a}_\infty$, respectively. All variables in Eq. (1) are nondimensionalized as follows:

$$\rho = \frac{\tilde{\rho}}{\tilde{\rho}_\infty} \quad p = \frac{\tilde{p}}{\tilde{\rho}_\infty \tilde{U}_\infty^2} \quad e = \frac{\tilde{e}}{\tilde{U}_\infty^2} \quad u, v = \frac{\tilde{u}, \tilde{v}}{\tilde{U}_\infty}$$

$$T = \frac{\tilde{T}}{\tilde{T}_\infty} \quad x, y = \frac{\tilde{x}, \tilde{y}}{\tilde{L}} \quad \mu = \frac{\tilde{\mu}}{\tilde{\mu}_\infty} \tag{2}$$

The ratio of the specific heats is denoted by γ and the viscosity is calculated using Sutherland's equation or by the power law. Perfect gas relations are used to close the above systems of equations. The nondimensional form of the equation of state is $T = \gamma M_\infty^2 p/\rho$.

Equation (1) is hyperbolic–parabolic with respect to the streamwise coordinate ξ, provided that the inviscid flow is everywhere supersonic, the streamwise velocity u is everywhere greater than zero, and a suitable technique is applied to the pressure term in the momentum equations to eliminate departure solutions. In this study the "Vigneron technique"[16] is used to avoid departure solutions. The Vigneron technique involves splitting $\boldsymbol{E}$ into two parts

$$\boldsymbol{E} = \boldsymbol{E}^* + \boldsymbol{P} \tag{3}$$

where

$$\boldsymbol{E}^* = \begin{bmatrix} \rho\bar{U} \\ \rho u\bar{U} + \left(\frac{\xi_x}{J}\right)\omega p \\ \rho v\bar{U} + \left(\frac{\xi_y}{J}\right)\omega p \\ \rho\bar{U}h \end{bmatrix}, \quad \boldsymbol{P} = (1-\omega)p\begin{bmatrix} 0 \\ \left(\frac{\xi_x}{J}\right) \\ \left(\frac{\xi_y}{J}\right) \\ 0 \end{bmatrix} \tag{4a}$$

and where ω is given by

$$\omega = \min\left[\frac{\sigma\gamma M_\xi^2}{1 + (\gamma-1)M_\xi^2}, 1\right] \tag{4b}$$

$\bar{U} = (\xi_x/J)u + (\xi_y/J)v$, and M_ξ is the Mach number in the streamwise direction. The entire pressure gradient is retained in the supersonic region while only a portion is retained in the subsonic region. The safety factor σ is used because the original eigenvalue analysis carried out by Vigneron was for a linear system.

III. Numerical Method

The PNS equations are integrated using a simple, explicit, finite volume, second-order-accurate algorithm. To develop a finite volume formulation Eq. (1a) is integrated over the arbitrary cell shown in Fig. 1. Applying Green's theorem reduces the surface integral to a line integral which is evaluated assuming flow properties are constant across each cell face. The net flux across the faces in the streamwise (ξ) direction is simply the difference in $\boldsymbol{E}_j^{n+1}$ and $\boldsymbol{E}_j^n$. The net cross-flow (η) flux is the difference in $\boldsymbol{F}_{j+1/2}^n$ and $\boldsymbol{F}_{j-1/2}^n$. The "$j \pm \frac{1}{2}$" denotes values at the interface between the j and $j \pm 1$ cells and n is the streamwise station. The discretized form of the PNS equations, assuming $\Delta\xi = \Delta\eta = 1$, is

$$\boldsymbol{E}_j^{n+1} - \boldsymbol{E}_j^n + (\boldsymbol{F}_{j+1/2}^n - \boldsymbol{F}_{j-1/2}^n) = 0 \tag{5}$$

Substituting Eq. (3) into Eq. (5) and linearizing the pressure term yields the final form of the discretized equations as

$$(\boldsymbol{E}_j^*)^{n+1} = (\boldsymbol{E}^*)^n - (\boldsymbol{F}_{j+1/2}^n - \boldsymbol{F}_{j-1/2}^n) - (\boldsymbol{P}_j^n - \boldsymbol{P}_j^{n-1}) \tag{6}$$

To avoid difficulty with stability, the pressure term in Eq. (6) is dropped.

To obtain second-order accuracy in the marching direction, we use a general two-step method[17] given as

$$\boldsymbol{E}^*(\boldsymbol{U}^p, \zeta^p) = \boldsymbol{E}^*(\boldsymbol{U}^n, \zeta^n) - \alpha\bar{\boldsymbol{F}}(\boldsymbol{U}^n, \zeta^n, \zeta^{n+1})$$

$$\boldsymbol{E}^*(\boldsymbol{U}^{n+1}, \zeta^{n+1}) = \boldsymbol{E}^*(\boldsymbol{U}^n, \zeta^n) - \beta\bar{\boldsymbol{F}}(\boldsymbol{U}^n, \zeta^n, \zeta^{n+1}) - \delta\bar{\boldsymbol{F}}(\boldsymbol{U}^p, \zeta^n, \zeta^{n+1}) \tag{7}$$

where $\bar{\boldsymbol{F}} = \boldsymbol{F}_{j+1/2} - \boldsymbol{F}_{j-1/2}$, $\zeta^p = \zeta^p(\xi + \chi\Delta\xi, \eta)$, and $\boldsymbol{U}$ is the matrix of dependent variables. ζ embodies geometry changes, and the other parameters are related to the accuracy parameter δ as $\beta = 1 - \delta$, $\alpha = \chi = \frac{1}{2}\delta$. By varying δ, we obtain the family of second-order schemes listed below with their commonly ascribed names:

$$\delta = \begin{cases} \frac{1}{2} \text{ Heun} \\ \frac{3}{4} \text{ Two-stage Runge-Kutta} \\ 1 \text{ Midpoint} \end{cases} \tag{8}$$

Experience has shown that $\delta = 1$ is the most accurate but least stable, and $\delta = \frac{1}{2}$ is least accurate but most stable, while $\delta = \frac{3}{4}$ is a compromise between the two.

Adaptive space-marching is used to predict the correct step size. The step size is computed from

$$\Delta x = \text{CFL} \min\left(\frac{1}{|\lambda_{\max}|}, Re_{\text{cell}}\right)\Delta d \tag{9}$$

Here, $\lambda_{\max}$ is the largest eigenvalue of the PNS system, Re_{cell} is the cell Reynolds number, CFL is the Courant, Friedrichs and Lewy stability number, and Δd is the distance of the first

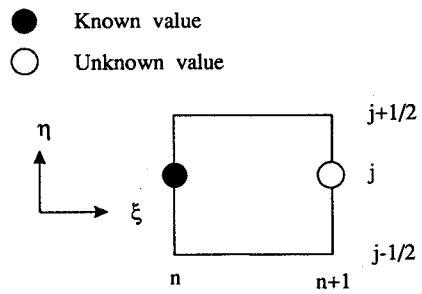

Fig. 1 Computational cell for finite volume formulation.

cell from the wall. When only the first step (first-order Euler integration) of the two-step algorithm is used, CFL is set to one, otherwise it is set to two. For strong shock/boundary-layer interaction CFL must be lowered.

A. Inviscid Flux

The inviscid fluxes are determined using the upwind schemes of Osher and Roe. These schemes belong to the subclass of upwind solvers referred to as Riemann solvers. Rather than solving the true Riemann problem, they use the solution to the approximate (linearized) Riemann problem to simplify the numerical algorithm. The inviscid flux of a cell in the η direction is given by

$$\boldsymbol{F}_i = (\eta_x/J)\, E_i + (\eta_y/J)\, F_i \tag{10}$$

The inviscid interface flux $\boldsymbol{H}_{j-1/2}$ may be represented as

$$\boldsymbol{H}_{j-1/2} = \frac{1}{2}\left(\boldsymbol{F}_i(\boldsymbol{U}_{j-1},\, \eta_{j-1/2}) + \boldsymbol{F}_i(\boldsymbol{U}_j,\, \eta_{j-1/2})\right) + \frac{1}{2}\int_{U_{j-1}}^{U_j} |\boldsymbol{A}(\boldsymbol{U},\, \eta_{j-1/2})|\, d\boldsymbol{U} \tag{11}$$

Where $\boldsymbol{A}$ is the flux Jacobian matrix defined as

$$\boldsymbol{A} = \boldsymbol{R}\Lambda\boldsymbol{R}^{-1},\ \Lambda = \mathrm{diag}(\lambda_m) \tag{12}$$

and $\boldsymbol{R}$ and $\boldsymbol{R}^{-1}$ are right and left eigenvectors, respectively, λ_m are the eigenvalues, and Λ is the diagonal matrix with λ_m as entries and η represents where the metrics are to be evaluated. The eigenvectors for Osher's scheme are associated with the Euler equations. Roe's scheme is more versatile since it is not restricted to use with the eigenvectors of the Euler equations. The eigenvectors have also been derived for the PNS system (see Appendix). The results computed using these two eigenvalue systems are compared in test case 3.

The manner in which the integral in Eq. (11) is evaluated is determined by which upwind scheme is used. For Roe's scheme specially averaged values of $\boldsymbol{U}$, designated as $\hat{\boldsymbol{U}}$, are used in defining an appropriate averaged value for $\boldsymbol{A}$, designated as $\hat{\boldsymbol{A}}$. The integral can then be represented as

$$\int_{U_{j-1}}^{U_j} |\boldsymbol{A}(\boldsymbol{U},\, \eta_{j-1/2})|\, d\boldsymbol{U} = |\hat{\boldsymbol{A}}(\hat{\boldsymbol{U}}_{j-1/2},\, \eta_{j-1/2})| \times (\boldsymbol{U}_j - \boldsymbol{U}_{j-1}) \tag{13}$$

Presently, no entropy-correction model is employed.

For Osher's scheme the integration path is split up into three subpaths. The subpaths are piecewise-parallel to the three eigenvectors which correspond to the three unique eigenvalues. The first and third subpaths correspond to the nonrepeated eigenvalues, while the second subpath corresponds to the repeated eigenvalue. The contribution of the three elementary disturbances (rarefaction wave, contact discontinuity, and compression wave) correspond to the integration along each of the three subpaths. The value of $\boldsymbol{U}$ along the subpaths reflects the contributions from the corresponding disturbances. The intersection of the subpaths are known as intermediate points. The eigenvalue along the first and third subpaths may change sign resulting in a sonic point. Once the value of $\boldsymbol{U}$ at the intermediate and sonic points is known, the integral in Eq. (11) is formally evaluated. The integral yields flux differences between cell values, intermediate values, and sonic values. For an ideal gas equation of state, the value of $\boldsymbol{U}$ at the intermediate and sonic points can be determined in closed form using Riemann invariants.

The present algorithm is second-order accurate in the crossflow and marching directions. The second-order crossflow flux is composed of the first-order flux and second-order spatial correction terms which are also TVD. TVD schemes provide a monotonic variation of flow properties which are second-order accurate. Two different models are used for the second-order inviscid flux-correction terms; the Chakravarthy and Osher[18] (C-O) limiter and the entropy-gradient[19] (E-G) limiter. Of course, TVD schemes such as these have only been proven theoretically for scalar nonlinear equations. However, the results obtained with second-order methods show substantial improvement over the first-order results, as illustrated in the second test case.

B. Boundary Conditions

For this space-marching algorithm, it is only necessary to apply boundary conditions at the upper and lower boundaries and supply a starting solution. The lower boundary is taken to be an isothermal or adiabatic solid wall where the velocity components are set to zero and the normal pressure gradient at the wall is assumed to be zero. The wall density is determined from the equation of state. The upper boundary is either a zero-gradient or a symmetry boundary. For the zero-gradient case, the flow variables are determined by extrapolation. For symmetry boundary, the dependent variables are reflected according to, $\boldsymbol{U}_{j\max} = \boldsymbol{S}\boldsymbol{U}_{j\max-1}$, where $\boldsymbol{S}$ is the identity matrix with -1 as the 3,3 entry.

The grids used in this study were constructed with an algebraic grid generator. Grid points were clustered along constant-ξ lines using Roberts[20] exponential stretching function.

IV. Numerical Results

To demonstrate the solution of the PNS equation using Osher's scheme, four two-dimensional, laminar test cases are presented. The first case models supersonic flow over a flat plate to emphasize the algorithms ability to accurately compute highly viscous flows. The second case, the supersonic diffuser, emphasizes the new methods capability to capture shock waves. The last two cases, hypersonic flow in a compression corner and hypersonic flow in an inlet, evaluate the ability of the algorithm to compute high-speed flows. In all cases, the solution was started from freestream conditions.

A. Test Case 1

This first case models supersonic laminar flow over a flat plate. The flow conditions are: $M_\infty = 2.0 - 5.0$; $Re_\infty = 1.65 \times 10^6$; $Pr = 0.70$; $\tilde{T}_\infty = \tilde{T}_w = 221.6$ K; and $\sigma = 0.80$. The plate supports a leading-edge shock and a Blasius-type profile. The grid, consisting of 95 points in the η direction, with an initial height of 0.06, was sized for each Mach number to capture the leading-edge shock. However, the spacing of the first cell off the wall was kept at a constant distance of 7.6250E-05. The solution was marched with an initial Δx of 0.125×10^{-4}. Once the Mach number of the first cell dropped to 0.75, adaptive space marching was initiated with a CFL of 2.0. Viscosity is computed from the power law with an exponent of 1.0. The C-O limiter is used with a compression parameter of $\frac{1}{3}$. Because the region of interest is highly viscous and no shocks were present, the solution was insensitive to changes in the accuracy parameter.

Four cases were computed by varying the Mach number between 2.0 and 5.0. The profile data were arbitrarily collected at $x = 0.93$. Results are compared with solutions found in Schlichting,[21] originally computed by Hantzsche and Wendt,[22] using the boundary-layer equations. Computations are made using both Roe and Osher upwinding. Velocity profiles are shown in Figs. 2a and 2b and temperature profiles are shown in Figs. 3a and 3b. The comparisons between the computations of Hantzsche and Wendt are in good agreement with the present computations, except for the maximum temperature which is about 3% low. Results for the two upwind methods are in excellent agreement as they appear as a single solid line in Figs. 2b and 3b.

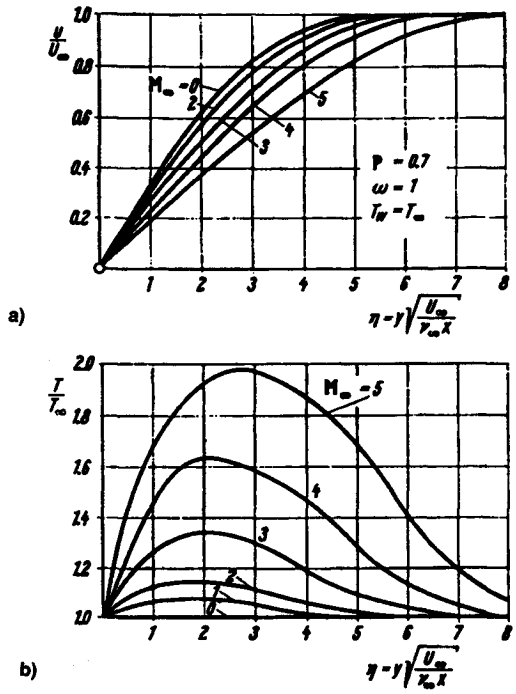

Fig. 2 Velocity profile on flat plate at zero incidence: a) after Hantzsche and Wendt[22]; b) computed with upwind solvers.

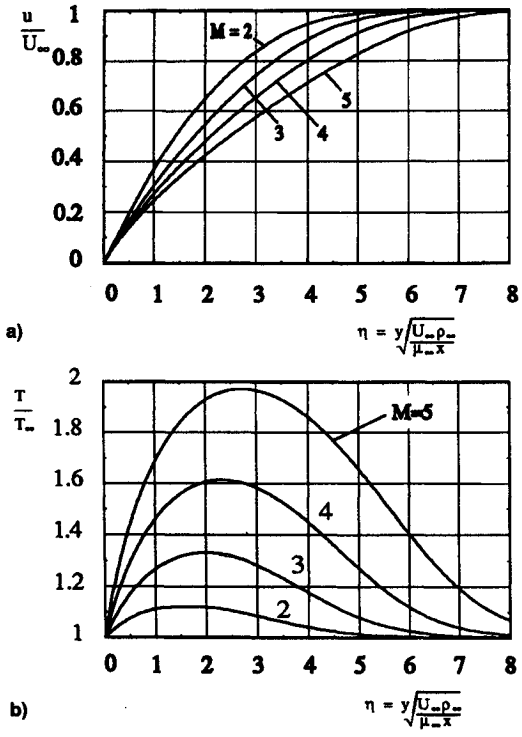

Fig. 3 Temperature profile on flat plate at zero incidence: a) after Hantzsche and Wendt[22]; b) computed with upwind solvers.

B. Test Case 2

This case models supersonic laminar flow in a diffuser. The flow conditions are: $M_\infty = 2.0$; $Re_\infty = 7.0 \times 10^6$; $Pr = 0.72$; $\tilde{T}_\infty = \tilde{T}_w = 419$ K; and $\sigma = 0.95$. The geometry for the case is shown in Fig. 4. The initial height of the grid 0.2 and the 5-deg wedge is located at $x = 0.2$. The combination of geometric parameters and initial conditions is such that the shock waves produced by the 5-deg wedge undergo regular reflections. The inviscid solution to this flow pattern can be approximated with two-dimensional oblique shock wave theory. The flow is modeled with a uniform grid of 60 points in the normal direction and a constant step size of 0.00025. The uniform grid and high Reynolds number minimize the effect of viscosity to provide better agreement with theoretical data. For the second-order results, δ was set to $\frac{3}{4}$ to capture shocks accurately, but with minimal oscillation in the entropy profiles. The C-O limiter was used with a compression parameter of $\frac{1}{3}$.

The theoretical results for static pressure ratio (p/p_∞) and entropy ratio (s/s_∞) are given for the 46th η cell. They are compared with first- and second-order Roe and Osher solutions. The comparisons for p/p_∞ and s/s_∞ are shown in Figs. 5 and 6, respectively. The upwind schemes are in good agreement with each other and with the theoretical results. There is a marked improvement in shock capturing going from first to second order (especially in entropy). With the finite volume formulation, the mass flux is conserved to machine zero.

C. Test Case 3

This test case models hypersonic laminar flow over a 15-deg wedge. The flow conditions were chosen to correspond to the experiment of Holden,[23] which has been studied extensively.[9,11,24–26] This flow is supersonic in the inviscid region and exhibits no separation of the boundary layer. The flow supports an extremely strong shock wave at the leading edge and a compression shock wave at the ramp. These features are shown in Fig. 7. The flow conditions are: $M_\infty = 14.1$; $Re_\infty = 1.04 \times 10^5$; $\tilde{L} = 0.439$ m; $Pr = 0.72$; $\tilde{T}_\infty = 72.2$ K; $\tilde{T}_w$

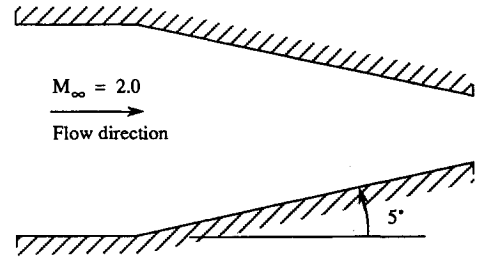

Fig. 4 Geometry for supersonic diffuser.

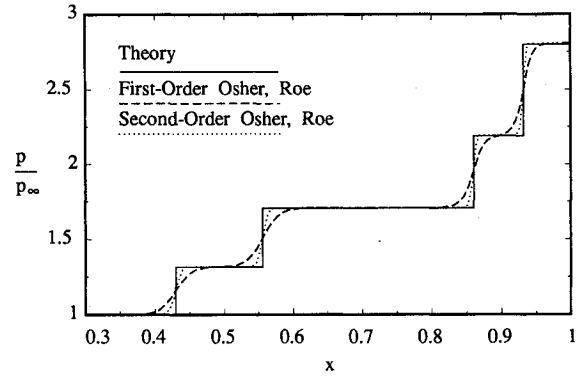

Fig. 5 Pressure ratio (p/p_∞) in supersonic diffuser.

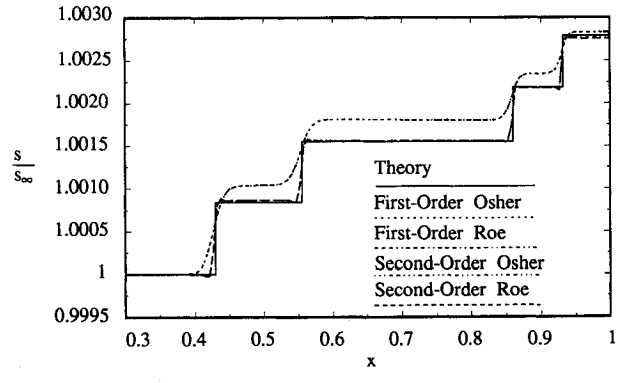

Fig. 6 Entropy ratio (s/s_∞) in supersonic diffuser.

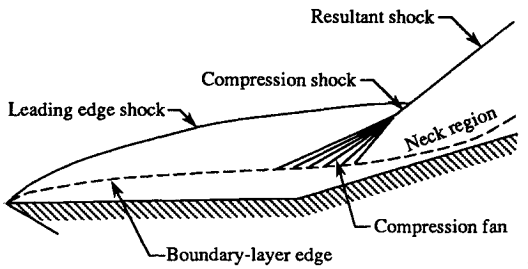

Fig. 7 Flow features for hypersonic ramp.

= 297 K; and $\sigma = 0.80$. The flow was modeled with 45 points in the η direction clustered near the wall with a stretching parameter of 1.08. The top of the grid was defined by

$$y = \begin{cases} 0.1708 + 0.0910x, & \text{if} \quad x < 1.66 \\ -0.2507 + 0.3445x, & \text{otherwise} \end{cases} \tag{14}$$

The solution was started with a step size of 1.7×10^{-4} and switched to adaptive marching when the Mach number of the first cell dropped to 0.75. CFL was set to 1.0 for first-order solutions and 2.0 for second-order solutions. For second-order results δ was set to $\frac{3}{4}$ and the E-G limiter was used with a compression parameter of 1.5. The E-G limiter was chosen, because it gave slightly better results than the C-O limiter.

Pressure, heat transfer, and skin friction coefficients are compared to the experimental values of Holden. The wall pressure coefficient C_p, heat transfer coefficient C_h, and skin friction coefficient C_f are defined as

$$C_p = \frac{p_{\text{wall}}}{\rho_\infty U_\infty^2}$$

$$C_h = \frac{\mu_{\text{wall}}}{PrRe_\infty} \frac{1}{\frac{1}{2}(\gamma - 1)M_\infty^2 + 1 - T_{\text{wall}}} \frac{\partial T}{\partial n}$$

$$C_f = \frac{\mu_{\text{wall}}}{Re_\infty} \frac{\partial T}{\partial n} \tag{15}$$

where n represents the normal distance from the wall. The comparison of C_p, C_h, and C_f with the experimental data is shown in Figs. 8, 9, and 10, respectively. The slight overprediction of values is consistent with previous investigators. The comparison of C_f shows no increase until after the ramp, because no information is propagated upstream to warn the flow of the ramp. Again, the agreement between the upwind schemes is good. The eigenvectors for the PNS system give similar results to the Euler system, although the stability limit is more restrictive. Thus, the use of the Euler eigenvectors instead of the PNS eigenvectors does not adversely affect the solution. The pressure contour for the second-order Osher scheme is shown in Fig. 11. Other contours are not shown because they are very similar.

D. Test Case 4

This final case is an extension of test 3; at the top of the ramp, the flow is expanded around a 15-deg wedge. The upper boundary is changed from a zero gradient extrapolation of test 3 to symmetric boundary conditions as in test 2. As the flow reaches the top of the ramp, the flow expands around the corner and the boundary layer thickens. The induced shock then intersects the boundary layer recompressing the flow. The strong shock/boundary-layer interaction and the reflected shock waves result in a demanding computational case. This case has also been studied extensively.[9,11,27,28] However, there are no experimental data and the solution is compared to the Navier-Stokes results of Deese and Agarwal.[28] The flow conditions are: $M_\infty = 15.0$; $Re_\infty = 8.0 \times 10^4$; $\tilde{L} = 0.4$ m; $Pr = 0.72$; $\tilde{T}_\infty = 100$ K; $\tilde{T}_w = 1000$ K; $\sigma = 0.80$.

This flow is modeled with 45 points in the η direction with a stretching parameter of 1.08. The solution was started with a step size of 1.875×10^{-4} and switched to adaptive space marching when the Mach number of the first cell dropped to 0.90. Before the solution reached the first shock boundary-layer region, CFL is dropped to 0.2 and then increased to 0.5

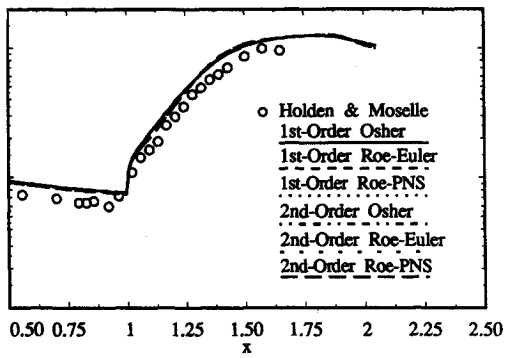

Fig. 8 Wall pressure coefficient for hypersonic ramp.

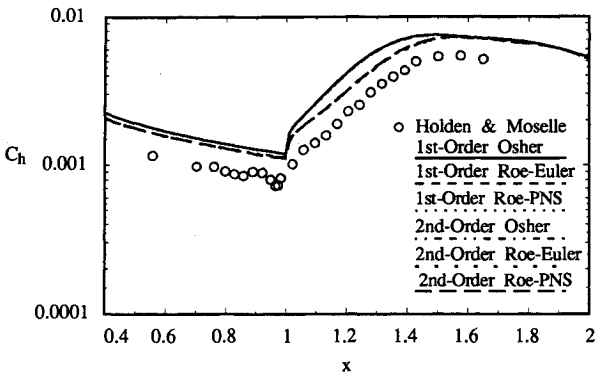

Fig. 9 Heat transfer coefficient for hypersonic ramp.

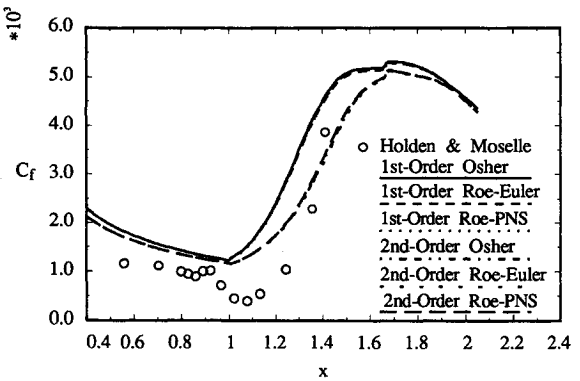

Fig. 10 Skin friction coefficient for hypersonic ramp.

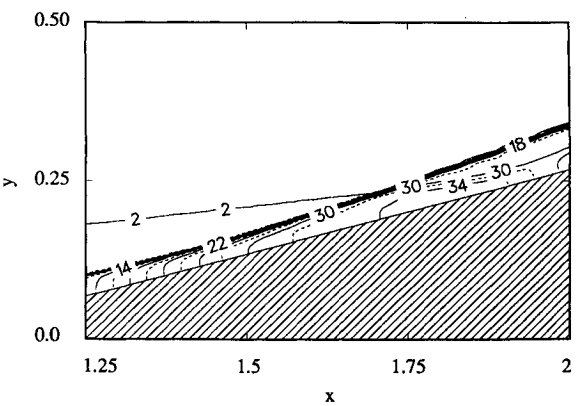

Fig. 11 Pressure contour for Osher scheme on hypersonic ramp.

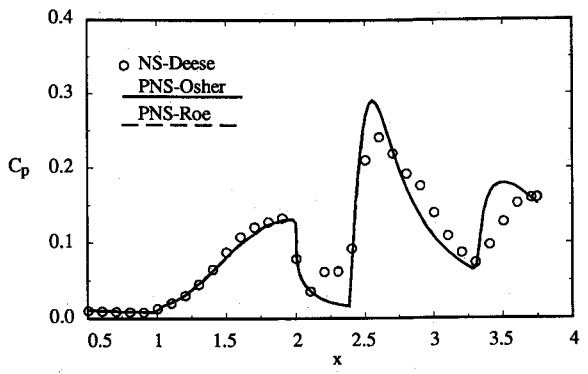

Fig. 12 Wall pressure coefficient for hypersonic inlet.

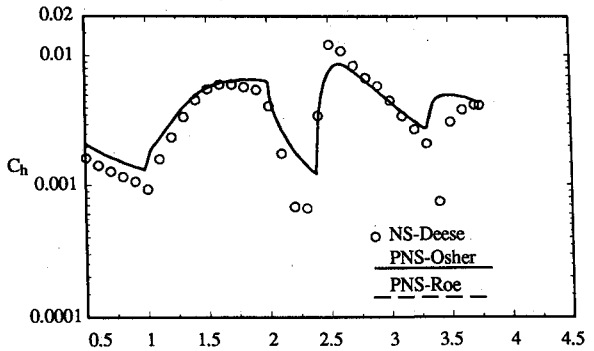

Fig. 13 Heat transfer coefficient for hypersonic inlet.

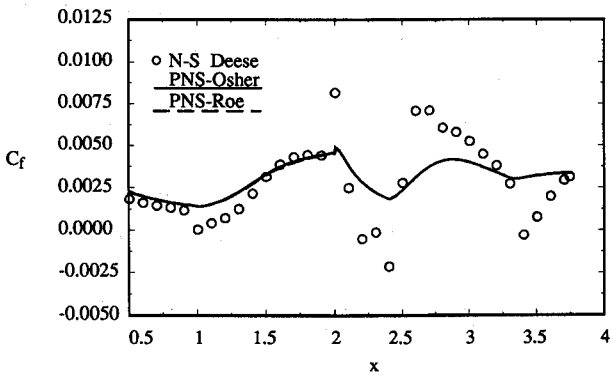

Fig. 14 Skin friction coefficient for hypersonic inlet.

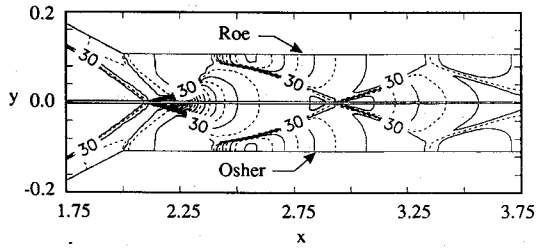

Fig. 15 Pressure contour for Osher and Roe schemes in hypersonic inlet.

before the second shock/boundary-layer interaction region. The C-O limiter was used with a compression parameter of $\frac{1}{3}$ and the accuracy parameter was set to $\frac{1}{2}$.

The C_p, C_h, and C_f coefficients are compared to the Navier-Stokes results in Figs. 12, 13, and 14, respectively. The discrepancy in the coefficients occurs because NS solvers[27,28] predict separation at the shock/boundary-layer interaction regions, while the PNS solvers march through these regions. The pressure profiles for Osher and Roe schemes are shown in Fig. 15, with the Roe solution on top and the Osher solution on bottom. Note that no oscillations in pressure occur in the boundary-layer region and that the contours agree well with each other.

Conclusion

A new, explicit, finite volume upwind PNS solver has been developed for high-speed flows which employs Osher and Roe upwinding. The algorithm is globally second-order accurate and employs flux limiters to make the solution TVD in the crossflow direction. The validity of the approach is demonstrated by computing four laminar-flow cases. The upwind solvers are able to crisply capture shocks and resolve highly viscous portions of the flowfield. Results agree well with theoretical and experimental results and other computations.

For the class of flows considered, no entropy correction model was necessary for Roe's scheme (no expansion shocks developed) and consequently the results agreed well with Osher's scheme. However, for three-dimensional flows with strong crossflow shocks, an entropy correction model may be necessary. Under those conditions, Osher's scheme should yield a more reliable solution. Osher's scheme was found to be more stable (a higher CFL may be used), but requires about 10% more CPU time to execute than Roe's scheme.

Employing the Euler eigenvectors, instead of the PNS eigenvectors, presents no difficulty in determining the crossflow flux. In fact, the Euler eigenvectors allow for a higher CFL. For flows without shock/boundary-layer interaction or only a mild interaction, the two formulations yield nearly identical results.

Work is currently underway[29] to extend the Osher solver to three dimensions and add a real-gas equation of state.

Appendix: Riemann Problem for PNS Equations

The interface flux is determined from the solution of the linearized Riemann problem. The Riemann problem can be solved using the unsteady problem associated with the Euler equations or the steady problem associated with the PNS equations. The Riemann problem associated with the Euler equations is given by

$$\frac{\partial \boldsymbol{U}}{\partial t} + \boldsymbol{A}_{j+1/2} \frac{\partial \boldsymbol{U}}{\partial \eta} = 0 \tag{A1}$$

where the matrix $\boldsymbol{A}_{j+1/2}$ is the Jacobian of the flux vector $\boldsymbol{F}$, with initial conditions

$$\boldsymbol{U} = \begin{cases} \left(\frac{1}{J}\right)_{j+1/2} \boldsymbol{U}_{j+1} & \text{if} \quad \eta > \eta_{j+1/2} \\ \left(\frac{1}{J}\right)_{j+1/2} \boldsymbol{U}_{j} & \text{if} \quad \eta < \eta_{j+1/2} \end{cases} \tag{A2}$$

for the $j + \frac{1}{2}$ cell interface.

The Riemann problem associated with the PNS equations is given by

$$\frac{\partial \boldsymbol{E}^*}{\partial \xi} + \boldsymbol{D}_{j+1/2} \frac{\partial \boldsymbol{E}^*}{\partial \eta} = 0 \tag{A3}$$

with initial conditions

$$\boldsymbol{E}^* = \begin{cases} \boldsymbol{E}^*(\boldsymbol{U}_{j+1}, \eta_{j+1/2}) & \text{if} \quad \eta > \eta_{j+1/2} \\ \boldsymbol{E}^*(\boldsymbol{U}_{j}, \eta_{j+1/2}) & \text{if} \quad \eta < \eta_{j+1/2} \end{cases} \tag{A4}$$

for the $j + \frac{1}{2}$ cell interface. The matrix $\boldsymbol{D}_{j+1/2}$ is of the form

$$\boldsymbol{D}_{j+1/2} = \left(\frac{\partial \boldsymbol{F}}{\partial \boldsymbol{E}^*}\right)_{j+1/2} \tag{A5}$$

The eigenvalues of $\boldsymbol{D}_{j+1/2}$, obtained from the solutions of $\det[\boldsymbol{A} - \lambda \hat{\boldsymbol{A}}^*] = 0$, where the inviscid flux Jacobian $\boldsymbol{A}^*$ is $\partial \boldsymbol{E}^*/\partial \boldsymbol{U}$, are

$$\lambda_{2,3} = \bar{V}/\bar{U}, \quad \lambda_{1,4} = (-a_2 \mp \sqrt{a_2^2 - 4a_1a_3})/2a_1 \tag{A6}$$

where the coefficients are given by

$$a_1 = \bar{U}^2\vartheta - c^2\omega k_\xi^2$$

$$a_2 = -\bar{U}\bar{V}(1+\vartheta) + (\omega+1)c^2\left(\frac{\xi_x}{J}\frac{\eta_x}{J} + \frac{\xi_y}{J}\frac{\eta_y}{J}\right)$$

$$a_3 = \bar{V}^2 - c^2 k_\eta^2 \tag{A7}$$

and

$$\bar{V} = u\frac{\eta_x}{J} + v\frac{\eta_y}{J}, \quad \bar{U} = u\frac{\xi_x}{J} + v\frac{\xi_y}{J}$$

$$c^2 = (\gamma-1)(h - \tfrac{1}{2}\phi^2)$$

$$\vartheta = \omega + \gamma(1-\omega), \quad k_\xi^2 = \left(\frac{\xi_x}{J}\right)^2 + \left(\frac{\xi_y}{J}\right)^2$$

$$k_\eta^2 = \left(\frac{\eta_x}{J}\right)^2 + \left(\frac{\eta_y}{J}\right)^2, \quad \phi^2 = u^2 + v^2 \tag{A8}$$

The matrix of right eigenvectors for $\boldsymbol{D}_{j+1/2}$, in $\Delta\boldsymbol{U}$ space, found from the solution of $[\boldsymbol{A} - \lambda_j\boldsymbol{A}^*]R_j = 0$, is

$$\boldsymbol{R} = \begin{bmatrix} 1 & 1 & 0 & 1 \\ u - \alpha_4(\lambda_1)\zeta(\lambda_1) & 0 & u & u - \alpha_4(\lambda_4)\zeta(\lambda_4) \\ v - \alpha_5(\lambda_1)\zeta(\lambda_1) & 0 & v & v - \alpha_5(\lambda_4)\zeta(\lambda_4) \\ h - \alpha_1(\lambda_1)\zeta(\lambda_1) & \dfrac{-\phi^2}{2} & \phi^2 & h - \alpha_1(\lambda_4)\zeta(\lambda_4) \end{bmatrix} \tag{A9}$$

where

$$\alpha_1(z) = \bar{V} - z\bar{U}, \quad \alpha_2(z) = \frac{\eta_x}{J} - z\frac{\xi_x}{J}$$

$$\alpha_3(z) = \frac{\eta_y}{J} - z\frac{\xi_y}{J}, \quad \alpha_4(z) = \frac{\eta_x}{J} - z\omega\frac{\xi_x}{J}$$

$$\alpha_5(z) = \frac{\eta_y}{J} - z\omega\frac{\xi_y}{J}$$

$$\zeta(z) = \alpha_1(z)/[\alpha_2(z)\alpha_4(z) + \alpha_3(z)\alpha_5(z)] \tag{A10}$$

Acknowledgment

This research was conducted under the McDonnell Douglas Independent Research and Development program.

References

[1]Engquist, B., and Osher, S., "One Sided Difference Approximations for Nonlinear Conservation Laws," *Mathematics of Computation,* Vol. 36, 1981, pp. 321–352.

[2]Roe, P. L., "Approximate Riemann Solvers, Parameter Vectors, and Difference Schemes," *Journal of Computational Physics,* Vol. 43, 1981, p. 357–372.

[3]Steger, J. L., and Warming, R. F., "Flux Vector Splittings of the Inviscid Gasdynamic Equations with Application to Finite Difference Methods," *Journal of Computational Physics,* Vol. 40, 1981, p. 263.

[4]van Leer, B., *Journal of Computational Physics,* Vol. 23, 1977, pp. 263–275.

[5]Anderson, W. K., Thomas, J. L., and van Leer, B., "Comparison of Finite Volume Flux Vector Splittings for the Euler Equations," *AIAA Journal,* Vol. 24, 1986, pp. 1453–1460.

[6]Osher, S., and Chakravarthy, S., "Upwind Schemes and Boundary Conditions with Applications to Euler Equations in General Geometries," *Journal of Computational Physics,* Vol. 50, 1983, pp. 447–481.

[7]Vinokur, M., "An Analysis of Finite-Difference and Finite-Volume Formulations of Conservative Laws," NASA CR-177416, June 1986.

[8]Roe, P. L., "Some Contributions to the Modeling of Discontinuous Flows," *Lectures in Applied Mathematics,* Vol. 22, 1985, p. 163.

[9]Lawrence, S. L., Tannehill, J. C., and Chaussee, D. S., "An Upwind Algorithm for the Parabolized Navier-Stokes Equations," AIAA Paper 86-1117, May 1986.

[10]Lawrence, S. L., Chaussee, D. S., and Tannehill, J. C., "Application of an Upwind Algorithm to the Three-Dimensional Parabolized Navier-Stokes Equations," AIAA Paper 87-1112, June 1987.

[11]Korte, J. J., and McRae, D. S., "Explicit Upwind Algorithm for the Parabolized Navier-Stokes Equations," AIAA Paper 88-0716, Jan. 1988.

[12]Korte, J. J., and McRae, D. S., "Numerical Simulation of Flow Over a Hypersonic Aircraft Using An Explicit Upwind PNS Solver," AIAA Paper 89-1829, June 1989.

[13]Yee, H. C., "A Class of High-Resolution Explicit and Implicit Shock-Capturing Methods," NASA TM-101088, Feb. 1989.

[14]Harten, A., "On a Class of High Resolution Total-Variation-Stable Finite-Difference Schemes," *SIAM Journal of Numerical Analysis,* Vol. 31, 1984, pp. 1–23.

[15]Osher, S., and Chakravarthy, S., "Upwind Schemes and Boundary Conditions with Applications to Euler Equations in General Geometries," *Journal of Computational Physics,* Vol. 50, 1983, pp. 447–481.

[16]Vigneron, Y. C., Rakich, J. V., and Tannehill, J. C., "Calculation of Supersonic Viscous Flow over Delta Wings with Sharp Subsonic Leading Edges," AIAA Paper 78-1137, July 1978.

[17]Gear, C. W., *Numerical Initial Value Problems in Ordinary Differential Equations,* Prentice-Hall, Englewood Cliffs, NJ, 1971, pp. 27–31.

[18]Chakravarthy, S. R., and Osher, S., "A New Class of High Accuracy TVD Schemes for Hyperbolic Conservation Laws," AIAA Paper 85-0363, Jan. 1985.

[19]Chakravarthy, S. R., and Osher, S., "High Resolution Applications of the Osher Upwind Scheme for the Euler Equations," AIAA Paper 83-1943, 1983.

[20]Anderson, D. A., Tannehill, J. C., and Pletcher, R. H., *Computational Fluid Dynamics and Heat Transfer,* 1st ed., Hemisphere, New York, 1984, p. 249.

[21]Schlichting, H., *Boundary-Layer Theory,* 7th ed., McGraw-Hill, New York, 1979, pp. 338–339.

[22]Hantzsche, W., and Wendt, H., "Die laminare Grenzschicht an der ebenen Platte mit und ohne Wärmeübergang unter Berücksichtigung der Kompressibilität," *Jb. det. Luftfahrtforschung I,* 1942, pp. 40–50.

[23]Holden, M. S., and Moselle, J. R., "Theoretical and Experimental Studies of the Shock Wave-Boundary Layer Interaction on Compression Surfaces in Hypersonic Flow," CALSPAN Rept. AF-2410-A-1, Oct. 1969.

[24]Gielda, T. P., and McRae, D. S., "An Accurate, Stable, Explicit, Parabolized Navier-Stokes Solver for High Speed Flows," AIAA Paper 86-1116, May 1986.

[25]Hung, C. M., and MacCormack, R. W., "Numerical Solutions of Supersonic and Hypersonic Laminar Compression Corner Flows," *AIAA Journal,* Vol. 14, 1976, pp. 475–481.

[26]Ng, W. F., Mitchell, C. H., Ajmani, K., Taylor, A. C., III, and Brock, J. S., "Viscous Analysis of High Speed Flows Using an Upwind Finite Volume Technique," AIAA Paper 89-0001, Jan. 1989.

[27]Newsome, R. W., Walters, R. W., and Thomas, J. L., "An Efficient Iteration Strategy for Upwind/Relaxation Solutions to the Thin-Layered Navier-Stokes Equations," AIAA Paper 87-1113, June 1987.

[28]Deese, J. E., and Agarwal, R. K., "Three-Dimensional Hypersonic Navier-Stokes Calculations Using Central-Difference Methods with Adaptive Dissipation," AIAA Paper 90-3069, Aug. 1990.

[29]Gerbsch, R. A., and Agarwal, R. K., "Solution of the Parabolized Navier-Stokes Equations for Three-Dimensional Real-Gas Flows Using Osher's Upwind Scheme," AIAA Paper 91-0248, Jan. 1991.